Photoabsorption studies of some closed-shell ions in the La isonuclear sequence

Sindhu Kalyadan, Hari R. Varma, P. C. Deshmukh, J. T. Costello, P. Hayden, and S. T. Manson

Phys. Rev. A **91**, 053422 — Published 26 May 2015

DOI: 10.1103/PhysRevA.91.053422

Photoabsorption studies of some closed-shell ions in the La isonuclear sequence

Sindhu Kalyadan[1], Hari R. Varma[1,*], P.C.Deshmukh[1, 2], J. T. Costello[3], P. Hayden[3] and S.T. Manson[4]

[1]School of Basic Sciences, Indian Institute of Technology Mandi, Mandi 175005, India
[2]Department of Physics and Astronomy, The University of Western Ontario, London N6G 3A9, Canada
[3]School of Physical Sciences, Dublin City University, Dublin 9, Ireland
[4]Department of Physics and Astronomy, Georgia State University, Atlanta, Georgia 30303, USA

*Corresponding author; hari@iitmandi.ac.in

Abstract

Photoionization cross sections and dipole angular distribution asymmetry parameters, β, of 5s and 4d shells of the closed-shell ions (La^{3+}, La^{9+} and La^{11+}) in the La isonuclear sequence have been studied using the relativistic random phase approximation (RRPA). The positions of the 5s Cooper minima in La^{3+} and La^{9+} ions are found to be extremely sensitive to the details of electron correlation. The results show that the 5s cross sections of $La^{3+}$and La^{9+} do not lie along the same curve near the thresholds; the 4d cross sections, however, do match well in overlap regions so they lie along the same curve, over the isonuclear sequence, except for a shift in threshold towards higher energies with increasing degree of ionization.

I. INTRODUCTION

A fundamental understanding of laser plasma emission and absorption mechanisms in the vicinity of 6.5 nm to 6.9 nm is important as spectral transitions in this region offer themselves as good candidates for next generation EUV lithography (EUVL) (so called 6.X nm lithography, or beyond EUV lithography (BEUVL)), due to the availability of high reflectivity (~60%) La/B_4C multilayer mirrors at these wavelengths [1]. Studies in this wavelength range could help determine the conditions for optimum conversion efficiency from a high power laser driver to 6.X nm wavelength plasma emission. This would be a key benchmark in determining the economic viability for deployment of any EUVL source solution in high volume manufacturing. Novel target configurations need to be explored towards gaining control in engineering plasma conditions to optimize the conversion efficiency, with transitions in Ag-, Pd- and Rh-like ion stages of Gd and Tb the most promising to date [2, 3]. We explore some ions amongst the lanthanides in an energy range overlapping with the energy region of interest for EUVL. We have chosen a few ions from the La isonuclear sequence to study their photoionization using the relativistic random phase approximation (RRPA), as La provides the material most suitable for producing high reflectivity multilayer mirrors for the next generation of EUVL and also La provides access to isoelectronic ion stages of the potential sources.

In addition, from a basic physics point of view, photoionization of multiply charged ions is of great interest in studying electron correlations and relativistic effects. Both resonant and non-resonant processes resulting from atomic/ionic photoabsorption are of interest [4]. Photoionization data are also very valuable in atmospheric physics, astrophysics, inertial confinement and tokomak fusion energy studies [5-9]. A number of photoionization measurements of outer shells of isonuclear sequences for Xe, Cs, Ba, Fe and Ce have been reported [10-14]. Theoretical calculations based on the Hartree-Slater and Dirac-Slater methods have been reported for the O, Fe, Hg isonuclear sequences [15-17]. Photoionization of the inner shells of the Mg, Ar and Ca isonuclear sequences [18-20] using the relativistic random phase approximation (RRPA) [21] have also been reported earlier. These studies showed that removal of electrons from a subshell having a higher principal quantum number does not have any effect on the inner shell photoionization cross sections, except for a shift in the photoionization

threshold to higher energies. However, along an isonuclear sequence, the angular distribution asymmetry parameter of the photoelectrons was found to show a different behavior near the thresholds due to its dependency on the Coulomb phase shift [20] which scales differently.

In the present work, we have chosen three multiply charged ions of the La (Z=57) isonuclear sequence. La^{3+}, La^{9+} and La^{11+} were chosen since they have closed-shell electron configurations and can therefore be studied using the RRPA [21]; the ground state structures of these ions are $[Kr]4d^{10}5s^25p^6$, $[Kr]4d^{10}5s^2$ and $[Kr]4d^{10}$, respectively. Photoionization of these ions is studied in the energy range 2.5 a.u. to 15 a.u. (ca. 70 – 400 eV or 18 to 3 nm respectively), which includes the region of current interest in the technology of next generation EUVL. EUV emission spectra of higher members of the La isonuclear sequence (La^{11+} to La^{20+}) have been reported in work by Kilbane and O'Sullivan [22]. They studied the transitions in the wavelength range 8.5 nm to 10.5 nm (5.4 a.u. to 4.4 a.u.) [22]. In this paper we report a study of photoionization cross sections as well as angular distribution parameters for 5s and 4d photoelectrons. These studies provide information about the energy range where bound-bound transitions can occur. In the present work, our focus is first on the study of the background (non-resonant) photoionization parameters; the autoionizing resonances will be studied separately using the Relativistic Multichannel Quantum Defect Theory (RMQDT) [23]. Photoionization of inner 4d shells for Xe like ions (Xe, Cs^+, Ba^{2+} and La^{3+}) using RRPA have been reported earlier [24]. The photoabsorption spectrum of La^{3+} ion in the 4d excitation region using the dual laser-produced plasma (DLP) technique has also been reported [25, 26].

II. THEORY

The Relativistic Random Phase Approximation (RRPA) [21] is a many-body theory, which includes electron correlations and relativistic effects. Electron correlations in the initial state of atomic photoionization process are built into the technique through time-backward ring diagrams (and corresponding exchange diagrams) over the Dirac-Hartree-Fock (DHF) wave functions and are essentially mixing of the initial state with two-particle two-hole excitation configurations. Correlations in the final state of the photoionization process are included through time-forward ring diagrams and amount to including interchannel coupling in the photoionization. The DHF threshold values used in our RRPA calculation are presented in Table 1. In the present work,

dipole channels arising from deep inner shells are omitted, and thus we have applied a truncation of the RRPA method, which results in small differences between the length and velocity forms of the transition matrix elements.

In the RRPA, the photoionization cross section for subshell (n,κ) is given by [21]

$$\sigma_{n,\kappa}(\omega)=\frac{4\pi^2\alpha\omega}{3}\left(\left|D_{nj\to j-1}\right|^2+\left|D_{nj\to j}\right|^2+\left|D_{nj\to j+1}\right|^2\right), \qquad \text{Eq. (1)}$$

where $D_{nj\to j'}$ represents the reduced dipole matrix element between an initial state orbital (n,κ_b) and a continuum orbital (ε,κ_b), and is given by [27]

$D_{nj\to j'}=i^{1-l}e^{i\delta_k}\left\langle\kappa\left|\left|Q_1^{(1)}\right|\right|\kappa_b\right\rangle$. Here δ_κ and l represent the phase shift and the orbital angular momentum quantum number of the continuum state respectively, while ω is the photon energy.

The dipole angular distribution asymmetry parameter β of the photoelectrons results from the interference between various electric dipole amplitudes [21] and is given by

$$\beta_{n\kappa}(\omega)=\left\{\begin{array}{l}\dfrac{(2j-3)}{2(2j)}\left|D_{j\to j-1}\right|^2-\dfrac{(2j-1)(2j+3)}{(2j)(2j+2)}\left|D_{j\to j}\right|^2+\dfrac{(2j+5)}{2(2j+2)}\left|D_{j\to j+1}\right|^2\\ -\dfrac{3}{2j}\left[\dfrac{(2j-1)}{2(2j+2)}\right]^{\frac{1}{2}}\left[D_{j\to j-1}D^*{}_{j\to j}+c.c\right]-\dfrac{3}{2}\left[\dfrac{(2j-1)(2j+3)}{2j(2j+2)}\right]^{\frac{1}{2}}\left[D_{j\to j-1}D^*{}_{j\to j+1}+c.c\right]\\ +\dfrac{3}{(2j+2)}\left[\dfrac{(2j+3)}{2(2j)}\right]^{\frac{1}{2}}\left[D_{j\to j}D^*{}_{j\to j+1}+c.c\right]\end{array}\right\}$$
$$\times\left\{\left|D_{j\to j-1}\right|^2+\left|D_{j\to j}\right|^2+\left|D_{j\to j+1}\right|^2\right\}^{-1}$$

Eq. (2)

where c.c. represents the complex conjugate.

To study the effects of interchannel coupling on the 5s photoionization in La^{3+} and La^{9+} in detail, several different levels of truncation of the RRPA calculations were performed to allow us to

pinpoint the effect(s) of each of the couplings. Specifically, the following truncations were utilized for each ion stage:

La^{3+} case:

(a) 2-channels: $5s_{1/2} \rightarrow p_{3/2}, p_{1/2}$

(b) 5-channels; $5s_{1/2} \rightarrow p_{3/2}, p_{1/2,} 4d_{3/2} \rightarrow p_{3/2}, p_{1/2}, f_{5/2}$

(c) 5-channels: $5s_{1/2} \rightarrow p_{3/2}, p_{1/2,} 4d_{5/2} \rightarrow p_{3/2}, f_{5/2}, f_{7/2}$

(d) 8-channels: $5s_{1/2} \rightarrow p_{3/2}, p_{1/2,} 4d_{5/2} \rightarrow p_{3/2}, f_{5/2}, f_{7/2,} 4d_{3/2} \rightarrow p_{3/2}, p_{1/2}, f_{5/2}$

(e) 13-channels: $5p_{3/2} \rightarrow d_{5/2}, d_{3/2}, s_{1/2}, 5p_{1/2} \rightarrow d_{3/2}, s_{1/2}, 5s_{1/2} \rightarrow p_{3/2}, p_{1/2}, 4d_{5/2} \rightarrow p_{3/2}, f_{5/2}, f_{7/2}, 4d_{3/2} \rightarrow p_{3/2}, p_{1/2}, f_{5/2}$

La^{9+} case:

(a) 2-channels: $5s_{1/2} \rightarrow p_{3/2}, p_{1/2}$

(b) 5-channels; $5s_{1/2} \rightarrow p_{3/2}, p_{1/2,} 4d_{3/2} \rightarrow p_{3/2}, p_{1/2}, f_{5/2}$

(c) 5-channels: $5s_{1/2} \rightarrow p_{3/2}, p_{1/2,} 4d_{5/2} \rightarrow p_{3/2}, f_{5/2}, f_{7/2}$

(d) 8-channels: $5s_{1/2} \rightarrow p_{3/2}, p_{1/2,} 4d_{5/2} \rightarrow p_{3/2}, f_{5/2}, f_{7/2,} 4d_{3/2} \rightarrow p_{3/2}, p_{1/2}, f_{5/2}$

La^{11+} case:

6-channels: $4d_{5/2} \rightarrow p_{3/2}, f_{5/2}, f_{7/2}, 4d_{3/2} \rightarrow p_{3/2}, p_{1/2}, f_{5/2}$.

III. RESULTS AND DISCUSSION

The 5s photoionization cross sections for the La^{3+} ion, calculated using the RRPA with different levels of truncation, are shown in Figs. 1(a) and 1(b) for the threshold and intermediate energy regions, respectively; the region between 3 and 5.2 a.u. is omitted as it is dominated by resonances. The 2-channel result does not include interchannel coupling with the photoionization cross sections from other subshells, and it shows a monotonic decrease from threshold. Since this result, although including interchannel coupling between $s \rightarrow p_{1/2}$ and $s \rightarrow p_{3/2}$ spin-orbit split continua, does not address correlations resulting from photoionization of the atom from other subshells, it is akin, to a significant extent, to what one may expect from a single-particle approximation. However, when

interchannel coupling with photoionization channels from other subshells are included, the result is significantly altered in the sense that the cross section does not exhibit the simple monotonic behavior as in the 2-channel result, as well as differences in the magnitude.

As seen in the Fig. 1(a), the two 5-channel ($5s+4d_{3/2}$ and $5s+4d_{5/2}$) results, the 8-channel (5s+4d) and the 13-channel (5p+5s+4d) results show an increase, if only a gentle one, of the cross section above threshold indicating that, with the coupling, the 5s Cooper minimum lies in the discrete region below the 5s threshold. In addition, Fig. 1(b) shows that both of the 5-channel coupled 5s cross sections, in which the truncated RRPA has employed interchannel coupling between the two relativistic dipole channels from the 5s with three relativistic dipole channels from either $4d_{5/2}$ or $4d_{3/2}$, shows an increase of the 5s cross section above the 4d thresholds, indicating the presence of an additional Cooper minimum below the 4d thresholds due to the coupling. The exact position of this second Cooper minimum is not shown in the figure, because background-photoionization parameters in this region are strongly modulated by the presence of autoionizing resonances resulting from the interference with 4d→ np, nf (bound—bound) resonances.

Figure 1(b) also shows the results of the 8-channel coupled truncated RRPA calculation in which dipole channels from the 5s, $4d_{3/2}$ and $4d_{5/2}$ subshells are included. The 8-channel result has an additional correlation beyond that addressed in the two separate 5-channel calculations, ($5s+4d_{3/2}$ and $5s+4d_{5/2}$). The Cooper minimum hinted at in the two separate 5-channel calculations now moves to higher energy, above the 4d thresholds, and is seen at ~ 6.25 a.u. indicated by the arrow in Fig. 1(b). The interchannel coupling between channels from the spin-orbit split 4d levels thus has an interesting effect on the 5s cross section; it is responsible for moving the two separate 5-channel coupled result for the 5s Cooper minimum to a higher energy, above the 4d subshells. It is interesting to note from this result that not only is the correlation resulting from coupling of the 4d channels with those from the 5s important, but the interchannel coupling between the relativistic dipole channels from the spin-orbit split 4d subshell is also important in locating the 5s Cooper minimum above the 4d thresholds. The net effect is then somewhat similar to the 'spin-orbit-interaction activated interchannel coupling' (SOIAIC) effect [28], since the interchannel coupling between channels from the spin-orbit split subshells is crucial.

Inclusion of additional interchannel coupling with channels from the 5p subshells moves the position of this 'induced' Cooper minimum to a still higher energy (~6.4 a.u.), as seen in the result for the 13-channel truncated RRPA curve shown in Fig. 1(b). The actual position of the 5s Cooper minimum is, thus, found to be extremely sensitive to the correlations resulting from interchannel coupling with all of the photoionization channels arising from subshells with nearby thresholds; interchannel coupling with channels arising from deep inner shells have negligible effect, however.

In the dipole photoionization studies of several atoms (Mg, Ca, Ba, Sr, Hg) it was found that interchannel coupling shifts the position of the Cooper minimum to a lower photon energy [29, 30]. However, in a recent study of 3s photoionization of the Cl-ion [31], it was found that increasing the interchannel coupling shifted the position of the Cooper minimum to higher energy. The present case is similar.

It is well known that in the vicinity of a Cooper minimum, the dipole angular distribution asymmetry parameter, β, for a ns subshell deviates from its non-relativistic value of 2 [32, 33]. β_{5s} for La^{3+}, determined for the different levels of truncation in the RRPA, are shown in Figs. 2(a) and 2(b). As seen from Fig. 2(a), at all levels of truncation, including the 2-channel calculations, β_{5s} deviates from the non-relativistic value of 2 near the 5s threshold. The 2-channel result for β_{5s} approaches 2 with increasing photon energies, as seen in Fig. 2(b). This observation confirms that the 2-channel result does not suggest the presence of any additional Cooper minima above the threshold, in agreement with the conclusion drawn from the monotonic decrease in the 2-channel cross section, σ_{5s}. The deviation near the threshold is due to the presence of the Cooper minimum in the discrete region.

As the photon energy increases above the threshold, the two 5-channel coupled calculations ($5s+4d_{3/2}$, $5s+4d_{5/2}$) also show that β_{5s} approaches the value of 2, albeit more slowly than the 2-channel result. However, β_{5s} exhibits a different behavior when further interchannel coupling is introduced. Of great interest is the result for β_{5s} obtained by the interchannel coupling from 8-channels; those from the 5s, $4d_{3/2}$, and $4d_{5/2}$ subshells. Figure 2(b) shows a clear dip in β_{5s} at about 6.25 a.u., suggesting the occurrence of a second Cooper minimum, induced by interchannel coupling – not just between channels from 5s and $4d_{5/2}$ or $4d_{3/2}$, but by the spin-orbit interaction

activated interchannel coupling or SOIAIC effect caused by interchannel coupling between relativistic dipole channels from 5s, $4d_{5/2}$ and $4d_{3/2}$ [34]. As in the case of the 5s photoionization cross section, β_{5s} also shows that the interchannel coupling induced Cooper minimum moves to an even higher energy (~6.4 a.u.) when additional dipole channels (from the 5p subshell) are coupled. Thus, it is clear that interchannel coupling with all of the relativistic 5p and 4d photoionization channels is required to obtain quantitatively correct results for both the cross section and the asymmetry parameter.

Next we investigate La^{9+} which has a $5s^2$ closed shell ground state electron configuration, i.e., as compared to the La^{3+} ion, the six 5p electrons absent. The 5s photoionization cross sections for the La^{9+} ion, determined by different levels of truncation, are shown in Fig. 3. As in the case of La^{3+} σ_{5s}, the 2-channel calculations here also displays a monotonic decrease with increasing energy above the 5s threshold. However, the 5-channel ($5s+4d_{5/2}$) calculation shows an increase in the cross section above the threshold; the other 5-channel ($5s+4d_{3/2}$) calculation (not shown) behaves similarly. This again indicates the presence of a Cooper minimum in the discrete region. The 8-channel σ_{5s} exhibits a Cooper minimum at ~ 5.6 a.u., induced by spin-orbit activated interchannel coupling. The angular distribution asymmetry parameter for La^{9+} 5s photoionization is shown in Fig. 4. The results for β_{5s} corroborate the conclusion, stated above, that interchannel coupling between the 4d channels with each other and with those from 5s subshell induces a second above-threshold Cooper minimum. It is quite evident that, in this case too, interchannel coupling is crucial for a correct determination of the location of the Cooper minimum and, thereby, the photoionization cross section.

Earlier photoionization studies reported that, along an isonuclear sequence, inner shell cross sections remain unchanged, except for a shift in the ionization thresholds [15-17] as long as only electrons with higher principal quantum numbers were removed. In going from La^{3+} to La^{9+} the 5p electrons are removed and, since 5s photoionization is being studied, electrons of the same principal quantum number are being removed. Thus, we have extended the studies on 5s photoionization from La^{3+} (13-channels) and La^{9+} (8-channels) up to 10 a.u., shown in Figs. 5 and 6, for the cross section and angular distribution asymmetry parameter, respectively. Note that, in these figures, the data for La^{3+} between 3 and 5.2 a.u. represents an approximate background cross section in a region

that is dominated by resonances, as mentioned earlier. As seen from Fig. 5, the La^{3+} cross section curve does not coincide with that for the La^{9+} cross section at or above the threshold of the latter, as expected. The removal of the 5p electrons from La^{3+} has a significant effect on the 5s photoionization cross section, because the orbital size of the two subshells is roughly the same (determined primarily by principal quantum number) so that the screening of the 5s changes considerably in going from La^{3+} to La^{9+}. The positions of the Cooper minima in the 5s cross sections above the 4d thresholds in $La^{3+}$and La^{9+} occur at different energies, resulting in the two significant difference in the cross sections. On the other hand, although the angular distribution asymmetry parameter, β, for these two cases exhibit similar features; they are, however, rather different in detail, as shown by Fig. 6. The primary cause of the large difference in the β's for the two cases is the energy-dependence of the position of the Cooper minima.

Photoionization calculations have also been performed for the 4d subshells of La^{3+}, La^{9+} and La^{11+} and the results for the 4d photoionization cross sections (the sum of $4d_{5/2}$ and $4d_{3/2}$) for each of the ions are shown in Fig. 7. The outstanding feature of this comparison is that the 4d cross sections for La^{3+}, La^{9+} and La^{11+} are almost exactly the same, except for an increase in the ionization thresholds. Removal of electrons from the 5p subshell leading to the formation of La^{9+}, and from the 5p and 5s subshells to form La^{11+}does not make any significant difference in the 4d cross sections, as functions of photon energy, except for a shift of the respective thresholds to higher energies. This is because the charge density of the n=5 electrons that were removed approximate a spherical shell of negative charge, well outside the spatial extent of the 4d orbitals; and a spherical shell of negative charge exerts no force on charges in its interior; its only effect is to increase the potential inside by a constant amount which accounts for the shift in thresholds with increasing stage of ionization [15-17]. In addition, it is of note that the individual $4d_{5/2}$ and $4d_{3/2}$ cross sections each lie along the same curve (not shown), as a function of photon energy, not just the total 4d cross section.

The 4d cross sections for La^{9+} and La^{11+} are seen to increase slightly from their respective 4d thresholds. However, this increase in the cross section is not due to the centrifugal barrier, as one might suspect. There is no delayed maximum (shape resonance) in the continuum for the La^{3+} 4d cross section caused by the centrifugal potential barrier, similar to the absence of the same for Ba^{2+} [24, 35]; the attractive Coulomb potential here is strong enough to pull the shape resonance into the

discrete region of the 4d spectrum. The La^{3+} cross section goes through a Cooper minimum at ~7.5 a.u. and then merges with the profiles for La^{9+} and La^{11+} cross sections, as seen in Fig.7. The slight increase of the 4d cross sections above the thresholds in La^{9+} and La^{11+} can therefore be attributed to the "recovery" from their respective Cooper minima in the discrete region.

In earlier work on La^{3+} by Cheng and Johnson [24], where only the six dipole channels from $4d_{5/2}$ and $4d_{3/2}$ were coupled, the Cooper minimum in the 4d cross section was reported at ~6.98 a.u. Our 6-channel result (not shown) and 13-channel results show this Cooper minimum at a slightly higher energy (~7.5 a.u.); the slight difference is probably numerical, since we have used essentially the same code [21], the difference being only due to the somewhat finer energy grid size used in the present work.

The dipole angular distribution asymmetry parameter for the 4d subshell for the La isonuclear sequence, averaged over spin-orbit split states, is given by [32, 33]

$$\beta_{4d} = \frac{\sigma_{4d5/2}\ \beta_{4d5/2} + \sigma_{4d3/2}\ \beta_{4d3/2}}{\sigma_{4d5/2} + \sigma_{4d3/2}}. \qquad \text{Eq. (3)}$$

The calculated β's are shown in Fig. 8. For La^{3+}, the calculated value of β_{4d} at the Cooper minimum is -0.303, which is different from the result one would expect from the non-relativistic value of 0.2 [36]. The behavior of β_{4d} for the three ions in the threshold region is slightly different, but, with increasing photon energy, these differences become smaller and will disappear at high enough energies. This is because the Coulomb phase-shifts in the angular distribution asymmetry parameter depend on the photoelectron kinetic energy, not photon energy, and the asymptotic charge of the residual ion [36, 19]. At high enough energies, however, the Coulomb phase shifts become quite small and their effect on the β parameter is then negligible; i.e., the differences get smaller with increasing electron kinetic energy.

The branching ratios $4d_{5/2}$:$4d_{3/2}$ for La^{3+}, La^{9+} and La^{11+} are shown in Fig. 9 and, since they are ratios of cross sections that are the same for each ion, as a function of photon energy, it is evident that the branching ratios must also lie along the same curve as seen. For La^{3+}, below the 4d ionization thresholds of La^{9+} and La^{11+}, the branching ratio is smaller than the statistical value of 1.5, and it decreases to 1.12 at ~ 6.7 a. u., below the $4d_{5/2}$ Cooper minimum. The branching ratio

then increases sharply to about 1.62, at a photon energy of ~8.8 a. u., after which it starts to decrease again towards the statistical value of 1.5. The sharp increase near the Cooper minimum occurs because the $4d_{5/2}$ cross section reaches its minimum value at a lower photon energy than the $4d_{3/2}$ cross section, which is a consequence of the Cooper minimum in the $4d_{5/2}$ channel lying at a lower photon energy than for the $4d_{3/2}$. This is the manifestation of a general rule that, for Cooper minima arising from spin-orbit split states, the minimum for the higher *j*-state always occurs at lower photon energies [37]. In any case, since the 4d thresholds of La^{9+} and La^{11+} are well above the Cooper minima, the branching ratio's show only a minor departure from the statistical value for these ions.

IV. CONCLUSIONS

Theoretical studies of the photoionization of near-outer subshells of three ions of the La isonuclear sequence have demonstrated that correlation in the form of interchannel coupling is of great importance, even for rather highly-charged ions. This was found to be particularly true in the vicinity of Cooper minima in the dipole matrix elements where the inclusion of interchannel coupling is critical; in fact it was seen that interchannel coupling induced Cooper minima where none appear without the coupling.

It was also confirmed that the photoionization cross section of a given subshell was affected significantly by removal of outer shell electrons with the same principal quantum number, but essentially unaffected by the removal of electrons with higher *n* as was found in the past in other cases [15-17]. However, an extension to that phenomenology was found; with the introduction of relativistic interactions, it applies individually to each *j*-state of a spin-orbit split subshell, specifically $4d_{5/2}$ and $4d_{3/2}$ in the present work.

Finally, it was demonstrated that there were various near-threshold effects owing to the relativistic splitting of the thresholds in the 4d case. Furthermore, dramatic deviations of the β parameter from the non-relativistic value of 2 were found in broad energy regions around the Cooper minima. Thus, it is evident that, for accuracy in the calculation of photoionization parameters in this region of the Periodic Table, relativistic calculations must be employed.

Acknowledgments

This work was supported by the Department of Science and Technology (DST), Government of India under grant DST/INT/IRE/P-17/11. The EU FP7 IRSES Grant Agreement No. 318941, under the project Ultrafast Photonics-Processes and Interactions (UP-PI), facilitating exchange between DCU and IITM is acknowledged. STM was supported by the US DOE, Office of Chemical Sciences.

Subshell	La^{3+}	La^{9+}	La^{11+}
$1s_{1/2}$	1439.85	1443.652	1445.24
$2s_{1/2}$	233.835	237.585	239.13
$2p_{1/2}$	219.97	223.73	225.29
$2p_{3/2}$	204.74	208.49	210.05
3s	52.37	56.06	57.577
$3p_{1/2}$	46.50	50.186	51.713
$3p_{3/2}$	43.46	47.142	48.668
4s	11.97	15.55	16.985
$3d_{3/2}$	33.30	37.003	38.537
$3d_{5/2}$	32.66	36.36	37.894
$4p_{1/2}$	9.722	13.28	14.739
$4p_{3/2}$	9.070	12.62	14.076
$4d_{3/2}$	5.305	8.855	10.298
$4d_{5/2}$	5.190	8.738	10.180
5s	2.635	5.515	
$5p_{1/2}$	1.926		
$5p_{3/2}$	1.822		

Table 1: Calculated Dirac-Hartree-Fock (DHF) subshell binding energies in a.u.

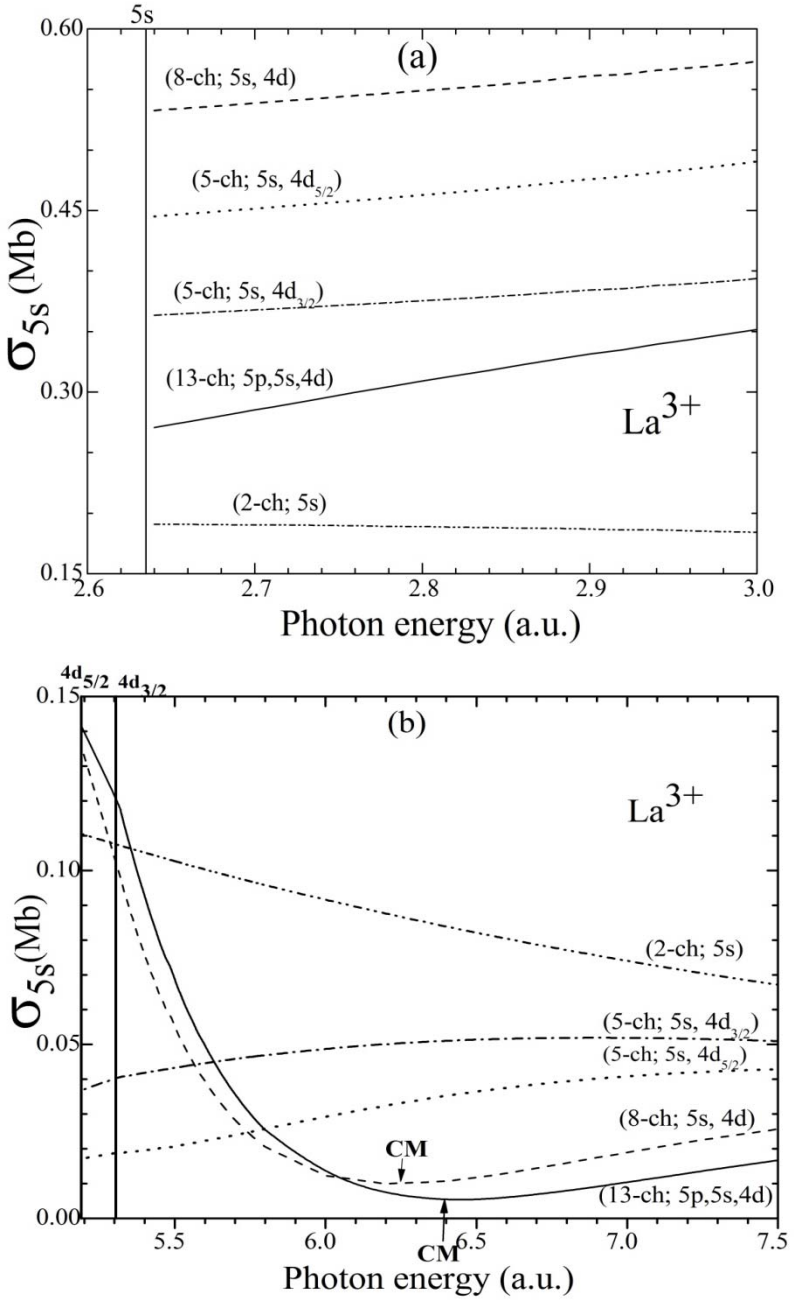

Figure 1. 5s photoionization cross sections, σ_{5s}, for La^{3+} calculated at various levels of truncation of the RRPA with each cross section labeled by the number of channels and the subshells included, and thresholds labeled and indicated by vertical lines for energies (a) 2.6 to 3.0 a.u., (b) 5.2 to 7.5 a.u. CM refers to the location of the Cooper minimum.

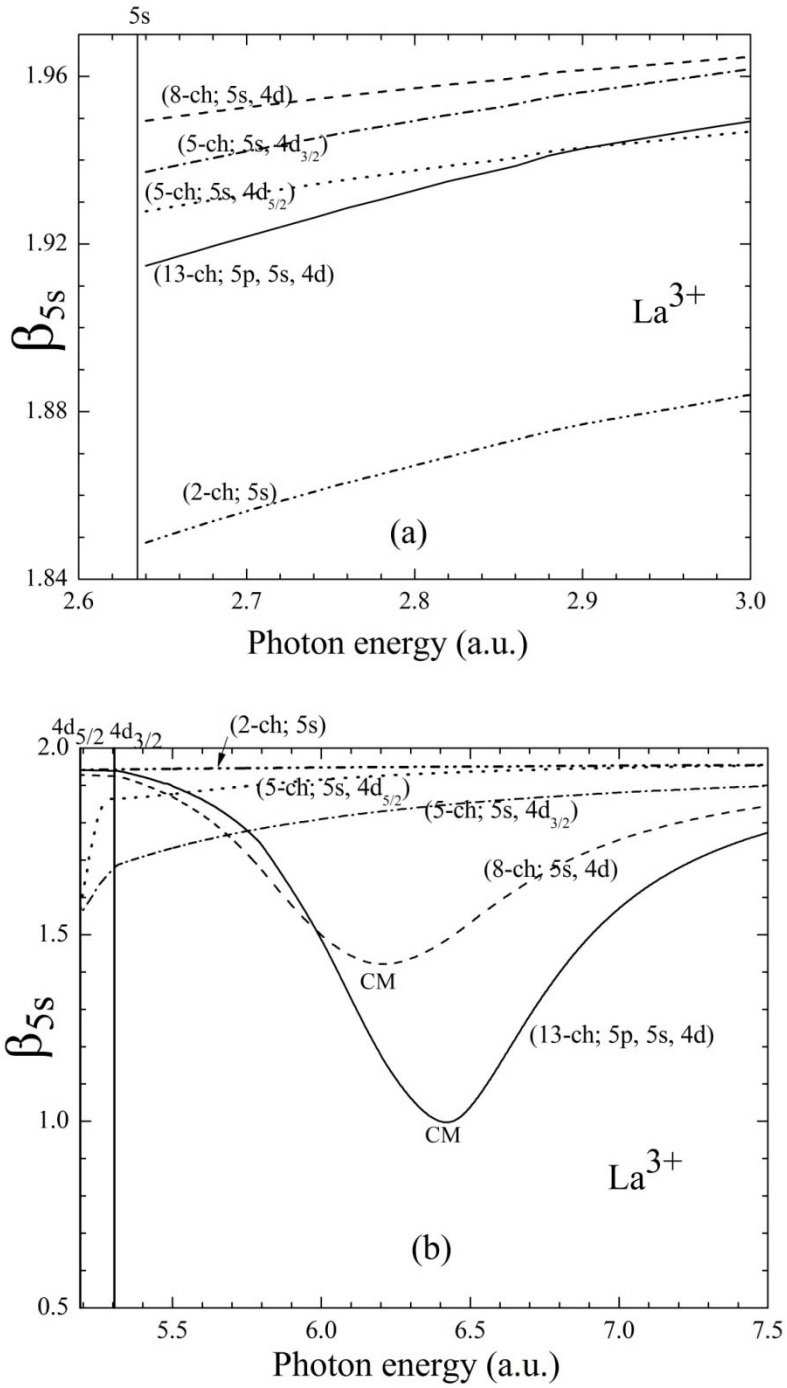

Figure 2. Same as Fig.1 but for the photoelectron angular distribution asymmetry parameter, β_{5s}

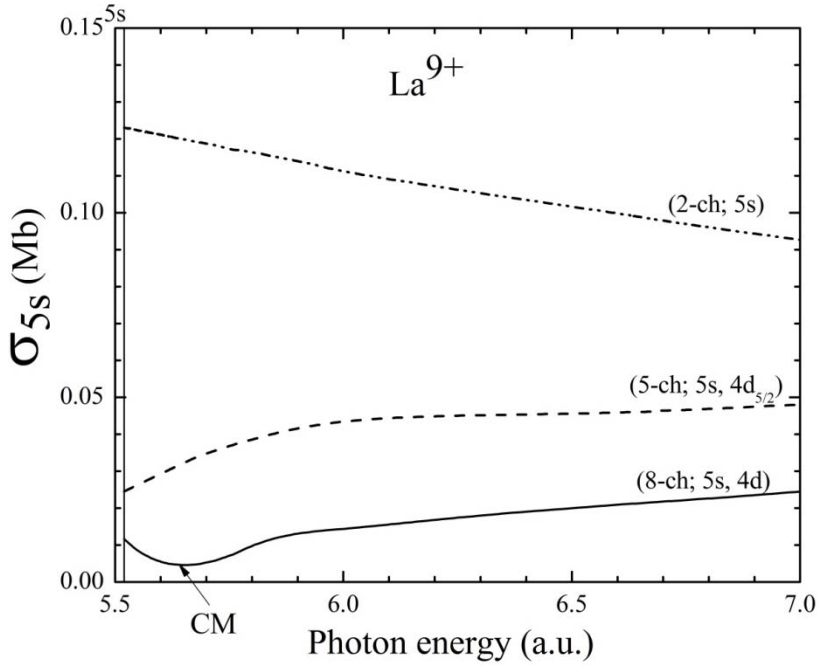

Figure 3.Same as Fig.1 but for La^{9+} in the 5.5 to 7.5 a.u. energy range

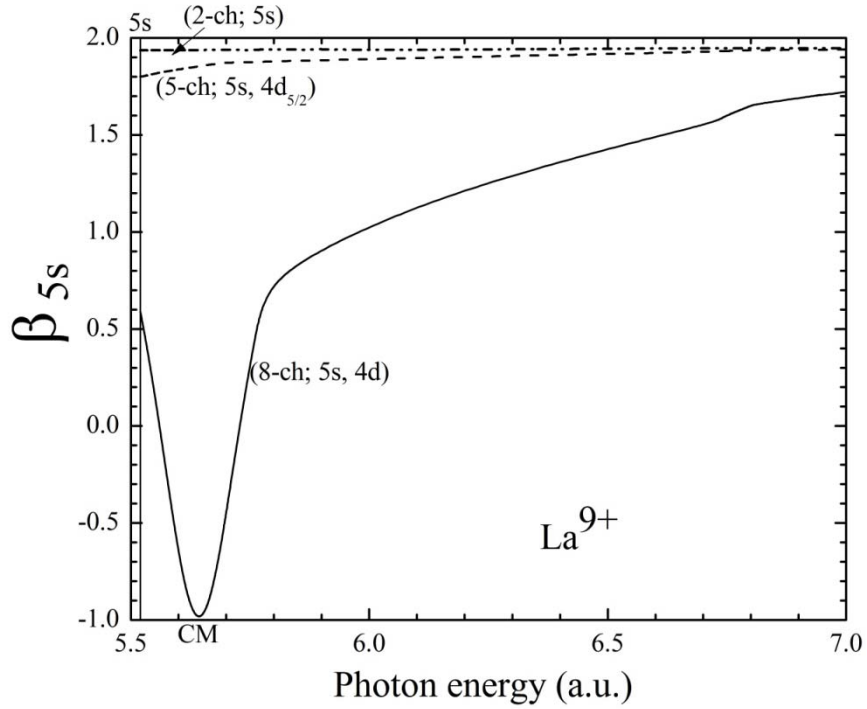

Figure 4. Same as Fig. 2 but for La^{9+} in the 5.5 to 7.5 a.u. energy range.

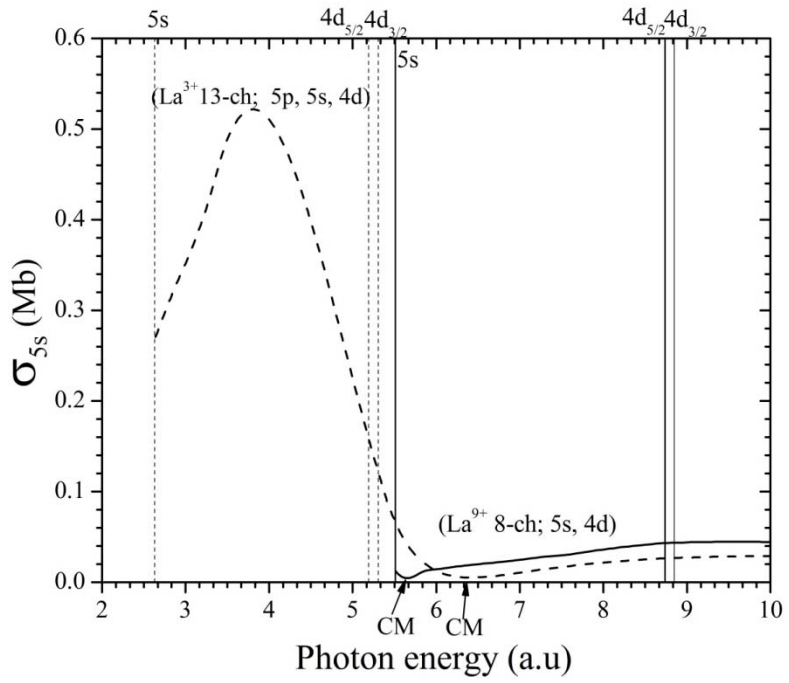

Figure 5. Same as Fig.1 but for La^{3+} and La^{9+}. The lower thresholds are for La^{3+} and the higher for La^{9+}.

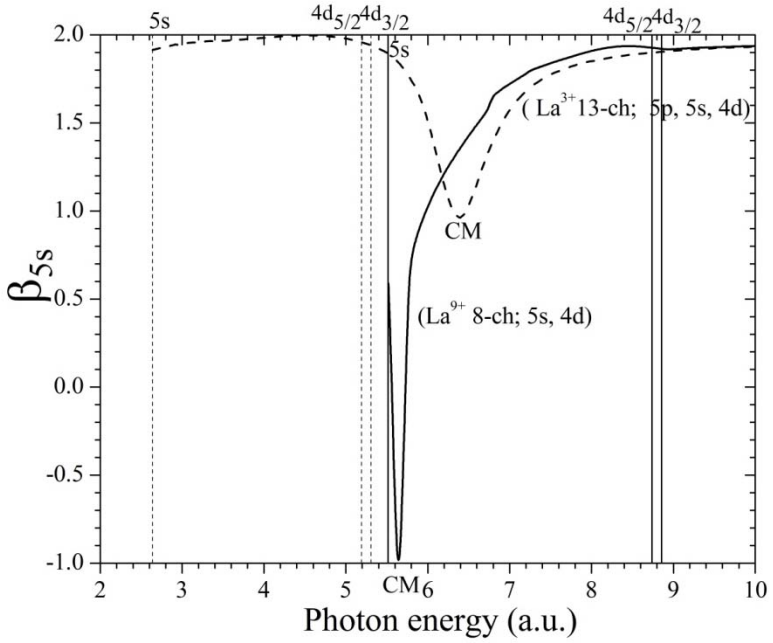

Figure 6. Same as Fig. 2 but for La^{3+} and La^{9+}. The lower thresholds are for La^{3+} and the higher for La^{9+}.

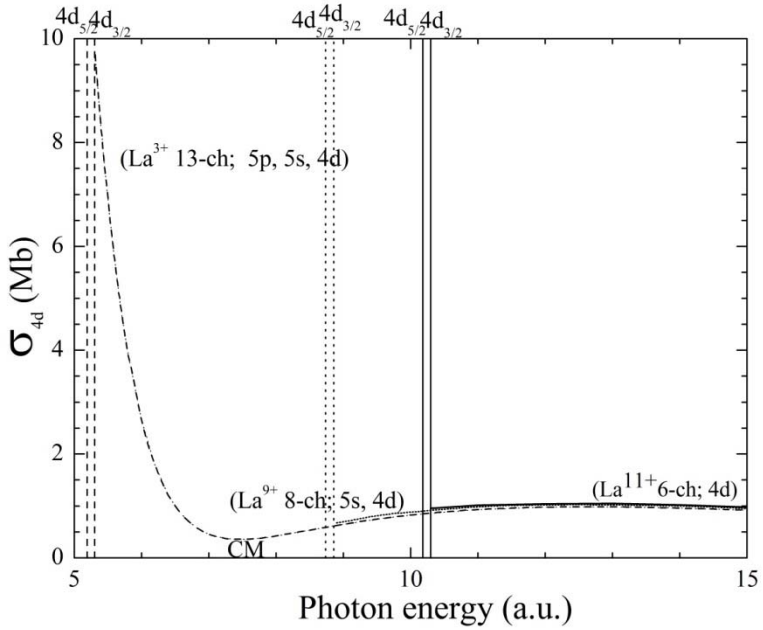

Figure 7. Same as Fig. 1 but for the total 4d cross sections ($4d_{5/2} + 4d_{3/2}$) of La^{3+}, La^{9+} and La^{11+}, with the 4d thresholds of each of the respective ion stages given.

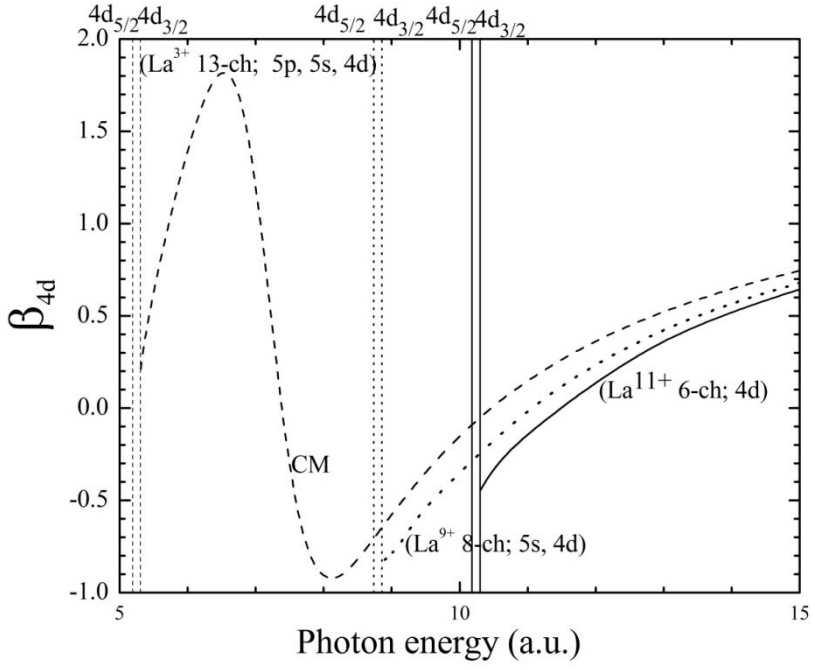

Figure 8. Same as Fig.2 but for the effective 4d β's of La^{3+}, La^{9+} and La^{11+} (as defined in text), with the 4d thresholds of each of the respective ion stages given.

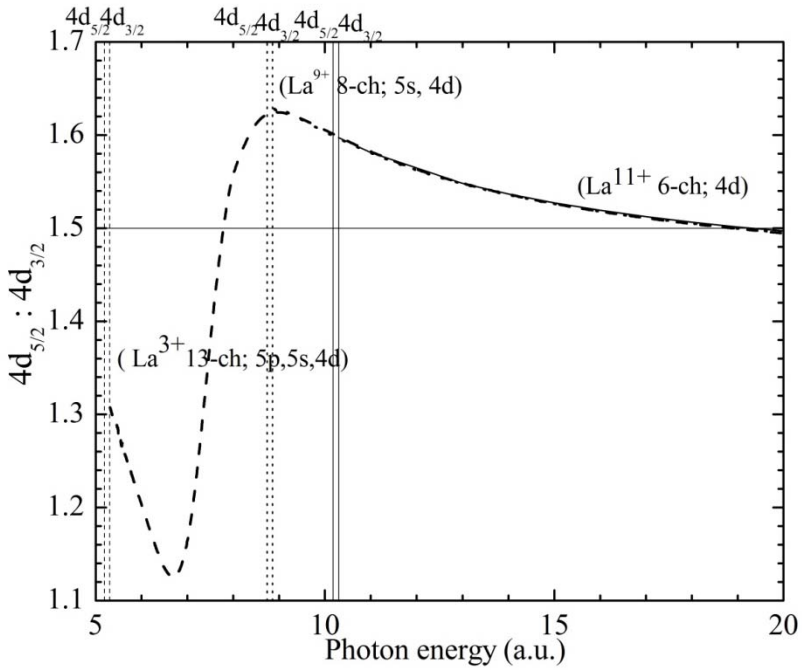

Figure 9: $4d_{5/2}$: $4d_{3/2}$ branching ratios for La^{3+}, La^{9+} and La^{11+} as functions of photon energy with the 4d thresholds of each of the respective ion stage given.

References

1. V. N. Polkovnikov, N. N. Salashchenko, S. D. Starikov and N. I. Chkhalo, Bull. Russ. Acad. Sci: Phys. **78**, 61 (2014).

2. B. Li, P. Dunne, T. Higashiguchi, T. Otsuka, N. Yugami, W. Jiang, A. Endo and G. O'Sullivan, Appl. Phys. Lett. **99**, 231502 (2011).

3. N. Tatsumura, S. Yamamura, T. Ozawa, K. Horioka, and T. Kawamura, Phys. Plasmas **20**, 083304 (2013).

4. J. -M. Bizau, J.-M. Esteva, D. Cubaynes, F. J. Wuilleumier, C. Blancard, A. Compant La Fontaine, C. Couillaud, J. Lachkar, R. Marmoret, C. Rémond, J. Bruneau, D. Hitz, P. Ludwig and M. Delaunay, Phys. Rev. Lett. **84**, 435 (2000).

5. Y. Y. Qi, Y. Wu and J. G. Wang, Phys. Plasmas **16**, 033507 (2009).

6. K. Davidson, Astrophys. J. **171,** 213 (1972).

7. J. Colgan, H. L. Zhang and C. J. Fontes, Phys. Rev. A **77**, 062704 (2008).

8. C. E. Theodosiou, S. T. Manson and M. Inokuti, Phys. Rev. A **34**, 943 (1986).

9. J. A. Shaw, M. S. Pindzola, M. Steidl, K. Aichele, U. Harten-Feller, D. Hathiramani, F. Scheuermann, M. Westermann and E. Salzborn, Phys. Rev. A **63**, 032709 (2001).

10. J. M. Bizau, C. Blancard, D. Cubaynes, F. Folkmann, J. P. Champeaux, J. L. Lemaire and F. J. Wuilleumier, Phys. Rev. A **73**, 022718 (2006).
11. A. Cummings, C. McGuinness, G. O'Sullivan, J. T. Costello, J. P. Mosnier and E. T. Kennedy, Phys. Rev. A **63**, 022702 (2001).
12. J. -M. Bizau, D. Cubaynes, J. -M. Esteva, F. J. Wuilleumier, C. Blancard, J. Bruneau, J. P. Champeaux, A. Compant La Fontaine, C. Couillaud, R. Marmoret, C. Rémond, D. Hitz, M. Delaunay, N. Haque, P. C. Deshmukh, H. -L. Zhou and S. T. Manson, Phys. Rev. Lett. **87**, 273002 (2001).
13. N. El Hassan, J. M. Bizau, C. Blancard, P. Cossé, D. Cubaynes, G. Faussurier and F. Folkmann, Phys. Rev. A **79**, 033415 (2009).
14. M. Habibi, D. A. Esteves, R. A. Phaneuf, A. L. D. Kilcoyne, A. Aguilar and C. Cisneros, Phys. Rev. A **80**, 033407 (2009).
15. D. W. Missavage, S. T. Manson and G. R. Daum, Phys. Rev. A **15**, 1001 (1977).
16. R. F. Reilmanand S. T. Manson, Phys. Rev. A **18**, 2124 (1998).
17. K. D. Chao and S. T. Manson, Phys. Rev. A **24**, 2481 (1981).
18. G. Nasreen, S. T. Manson and P. C. Deshmukh, Phys. Rev. A **40**, 6091 (1989).
19. G. B. Pradhan, J. Jose, P. C. Deshmukh, V. Radojević and S. T. Manson, Phys. Rev. A **81**, 063401(2010)
20. G. B. Pradhan, J. Jose, P. C. Deshmukh, V. Radojević and S. T. Manson, Phys. Rev. A **80**, 053416 (2009).
21. W. R. Johnson and C. D. Lin, Phys. Rev. A **20**, 964 (1979);
W. R. Johnson, C, D. Lin, K. T. Cheng and C. M. Lee C M, Phys. Scr. **21**,409 (1980).
22. D. Kilbane and G. O'Sullivan, Phys. Rev. A **82**, 062504 (2010).
23. C.M. Lee and W. R. Johnson, Phys. Rev. A **22,** 979(1980)
24. K. T. Cheng and W. R. Johnson, Phys. Rev. A **28**, 2820 (1983).
25. U. Köble, L. Kiernan, J. T. Costello, J. -P. Mosnier, E. T. Kennedy, V. K. Ivanov,
V. A. Kupchenkoand M. S. Shendrik, Phys. Rev. Lett. **74**, 2188 (1995).
26. N. Murphy, A. Cummings, P. Dunne and G. O'Sullivan, Phys. Rev. A **75**, 032509 (2007).
27. A. Derevianko, W. R. Johnson and K. T. Cheng, At. Data Nucl. Data Tables **73**, 153 (1999).
28. S. Sunil Kumar, T. Banerjee, P. C. Deshmukh and S. T. Manson, Phys. Rev. A **79**, 043401 (2009).

29. T. Banerjee, P. C. Deshmukh and S. T. Manson, Phys.Rev. A **75,** 042701 (2007).

30. H. R. Varma and P. C. Deshmukh, Photoabsorption Processes in Some Free and Confined Atomic Systems: Effects of Correlation, Relativistic Interactions and Confinement (Lambert Academic Publishing, Saarbrücken, Germany, 2011), Ph.D. Thesis, IIT-Madras.

31. J. Jose J, G. B. Pradhan, V. Radojević, S. T. Manson and P. C. Deshmukh J. Phys. B **44**, 195008 (2011).

32. T. E. H. Walker and J. T. Waber, Phys. Rev. Lett. **30**, 307 (1973).

33. S. T. Manson and A. F. Starace Rev. Mod. Phys. **54**, 389 (1982).

34. V. Radojević, M. Kutzner and H. P. Kelly, Phys. Rev. A **40**, 727 (1989).

35. T. B. Lucatorto, T. J. McIlrath, J. Sugar, and S. M. Younger, Phys. Rev. Lett. **47**, 1124 (1981).

36. S. T. Manson, J. Electron Spectrosc. Relat. Phenom. **37**, 37 (1985).

37. Y. S. Kim, A. Ron, R. H. Pratt, B. R. Tambe, and S. T. Manson, Phys. Rev. Lett.**46**, 1326 (1981)